J. Nanostruct Chem. 2026; 16(1): 38-55

Journal of Nanostructure in Chemistry (JNSC)

https://doi.org/10.57647/jnsc.2026.1601.03

Research Article

Biosynthesis of Silver Nanoparticles Using *Rhubarb* Seed Extract for the Effective Removal of Organic Dyes from Aqueous Media: Insights into Isotherm and Kinetics Models

Hamid Reza Heidari[1], Mohammad Yari[1,*], Sajjad Sedaghat[2], Masoumeh Sayadian[1], Vida Jodaian[1]

[1]*Department of Chemistry, Isl.C., Islamic Azad University, Islamshahr, Iran*
[2]*Department of Chemistry, ShQ.C., Islamic Azad University, Shahr-e Qods, Iran*
*
Corresponding authors: mohammadyari@iau.ac.ir

Article History:

Received:
11 October 2025

Revised:
27 November 2025

Accepted:
18 December 2025

Published in Issue:
28 February 2026

Abstract

Improper disposal of synthetic dyes like methylene blue (MB), methyl orange (MO), and acid red 18 (AR18) poses a significant threat to aquatic environments and human health, highlighting the need for efficient and sustainable remediation strategies. This study introduces a novel, green synthesis of silver nanoparticles (AgNPs) using *Rhubarb* seed extract. It provides a cost-effective, eco-friendly, and rapid method to produce functional adsorbents for treating dye-contaminated wastewater. Thorough characterization confirmed the morphology and composition of the biosynthesized AgNPs through UV-Vis spectroscopy, transmission electron microscopy (TEM), dynamic light scattering (DLS), scanning electron microscopy (SEM), energy-dispersive X-ray (EDX), Fourier transform infrared spectroscopy (FT-IR), and X-ray diffraction analysis (XRD). Batch adsorption experiments showed outstanding maximum removal efficiencies exceeding 95% for MB, MO, and AR18 under optimal conditions (pH 11, 9, and 5, respectively; 0.8 g adsorbent; 20 minutes contact time; 30 mg/L dye concentration). The adsorption process followed the Langmuir isotherm (R^2 = 0.9998 for MB, 0.9994 for MO, 0.9999 for AR18) and pseudo-second-order kinetics (R^2 = 0.9998, 0.9992, and 0.9991, respectively), with maximum adsorption capacities (q_{max}) of 40.16, 50.76, and 44.64 mg/g. The innovation of this research lies in using *Rhubarb* seed extract for AgNP biosynthesis, showcasing high performance even for complex dye mixtures while promoting environmental sustainability and economic viability compared to conventional chemical methods. These findings establish *Rhubarb* seed-derived AgNPs as an effective and innovative platform for advanced wastewater purification.

Keywords: Adsorption; Biosynthesis, Dye removal; *Rhubarb* seed extract; Silver nanoparticles (AgNPs)

Cite this article: Heidari, H. R., Yari, M., Sedaghat, S., Sayadian, M., Jodaian, V., Biosynthesis of Silver Nanoparticles Using *Rhubarb* Seed Extract for the Effective Removal of Organic Dyes from Aqueous Media: Insights into Isotherm and Kinetics Models. *J Nanostruct Chem* **16**, 38-55 (2026). https://doi.org/10.57647/jnsc.2026.1601.03

Highlights

• Green synthesis of AgNPs can be effectively achieved using *Rhubarb* seed extract as a natural reducing agent.
• The biosynthesized AgNPs demonstrate high efficiency in removing organic dyes from aqueous solutions.
• Detailed adsorption studies using isotherm models and kinetic models provide insights into the dye adsorption mechanisms and the interaction behavior between the dyes and the AgNPs.
• Characterization techniques confirm the successful synthesis of AgNPs with desirable size, morphology, and surface properties, which contribute to their effectiveness.

Graphical Abstract

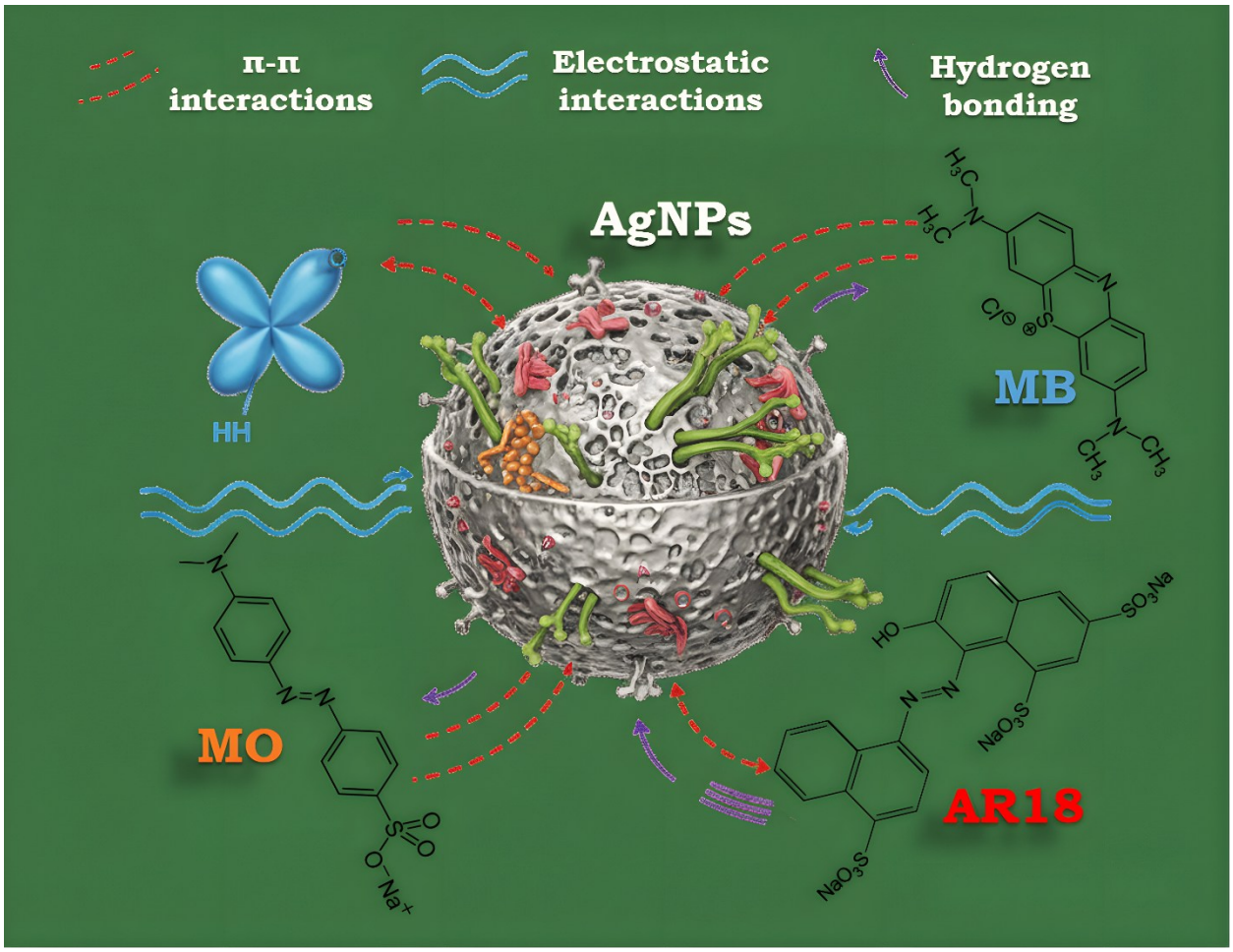

1. Introduction

Industrialization is increasing, resulting in the release of large amounts of industrial effluents containing toxic pollutants such as dyes, heavy metals, and pesticides into aquatic environments [1]. Many industries that widely use synthetic dyes include textiles, plastics, paper, leather, cosmetics, food products, and pharmaceuticals, which produce highly dye wastewater [2]. It has been estimated that the widespread use of different types of synthetic dyes has resulted in approximately 5,000–10,000 tons of dyes being released into waterways annually [3]. Methylene blue (MB) (Scheme 1a), also known as Swiss blue, is a cationic synthetic dye with a thiazine structure. It is used in the textile, leather, printing, pharmaceutical, and personal care industries [4,5]. Vomiting, nausea, anemia, permanent eye damage, breathing difficulties, tissue necrosis, and high blood pressure are common side effects of prolonged exposure to this dye. It is not highly toxic, but ingestion causes a burning sensation. Therefore, it is essential to eliminate MB from industrial wastewater prior to its release into water bodies [6,7]. Methyl orange (MO) (Scheme 1b) is categorized in the class of anionic dyes [8]. It is commonly used in the food, pharmaceutical, textile, paper, and printing industries [9,10]. Being soluble in water and resistant to degradation allows them to persist in the environment, posing a hazard to living organisms [11].The presence of MO in water prevents sunlight penetration, affecting

10.57647/jnsc.2026.1601.03

photosynthesis, reducing oxygen in ecosystems, and causing the death of aquatic organisms [12]. This dye poses multiple health risks, including elevated heart rate, carcinogenic and mutagenic effects, genotoxicity, vomiting, and even shock [13]. Acid Red 18 (AR18) (Scheme 1c), known as Cochineal Red A, Ponceau 4R, New Coccine, or E124, is a sulfonated azo dye. It is used in the pharmaceutical, cosmetics, and food industries [14,15]. Researchers have reported gastrointestinal discomfort, vomiting, cardiovascular shock, reproductive toxicity, mutagenic, neurobehavioral, and carcinogenic effects of azo dyes and intermediate products on human health and aquatic life [16-18]. Hence, eliminating AR18 from dye-contaminated wastewater prior to its release into aquatic ecosystems is crucial. Several techniques, such as coagulation [19], coagulation-flocculation [20], electrocoagulation [21,22], ozonation [23], and ultrafiltration [24], have been used to remove the aforementioned dyes from aqueous solutions. However, these methods have limitations, including the generation of sludge and disposal problems, low efficiency, high operational costs, and the creation of secondary contaminants due to the production of toxic chemical residues [25,26]. In contrast, one of the most efficient methods is adsorption, owing to its simple design, simplicity of the process, high efficiency, low cost, and reusability of the adsorbent [27-29].

Nanotechnology can produce nanomaterials that can be used for various environmental purposes. The small size (less than 10 nm) of the nanoparticles (NPs) and the high surface-to-volume ratio make them more reactive to interact with other molecules [30]. Metal NPs, such as gold (Au), silver (Ag), and zinc (Zn), have recently attracted the attention of researchers because of their unique features, such as high stability, large surface area, high efficacy, and facile chemical modification. Among them, silver nanoparticles (AgNPs) have been widely considered for their extensive range of applications owing to their well-known characteristics, such as chemical stability, antibacterial activity, thermal and electrical conductivity, and catalytic and optoelectronic properties [31,32].

AgNPs have been synthesized using physical and chemical methods, which present several drawbacks such as the use of harmful chemicals, expensive equipment, high pressure and temperature requirements, and the necessity for extensive space. To overcome these restrictions, green synthesis was introduced as an environmentally friendly and economical technique for the synthesis of NPs [33]. Green synthesis of NPs primarily relies on capping and reducing agents found within plant extracts. Plant extracts can be produced from different parts of the plant (stem, leaves, fruits, seeds, roots, and flowers.

Reducing agents, including phenols, membrane proteins, flavonoids, and other secondary metabolites, are present in these parts. Furthermore, plant extracts contain capping agents, such as peptides, tannic acids, and enzymes [34]. Biosynthesized AgNPs, used as adsorbents, offer significant advantages such as eco-friendly, cost-effective synthesis, high adsorption efficiency, and antimicrobial activity. These qualities enhance their utility in removing pollutants from water. The biomolecule capping on the nanoparticles stabilizes them, allowing for reusability and reducing aggregation [79].

However, they also have disadvantages, including potential nanotoxicity, limited selectivity in removing mixed contaminants, stability issues under varying conditions, cost factors related to silver, concerns about environmental release, and possible complexity in regeneration after repeated use. Overall, they present a promising but carefully managed solution for sustainable adsorption applications [80].

Biosynthesized AgNPs using green way show antibacterial against gram-positive and gram-negative bacteria, antifungal, antioxidant, anticancer, medical diagnostics, therapeutic, and cytotoxic properties, as well as catalytic activities for the reduction of organic dyes [35-37]. In other hand, AgNPs induce cytotoxicity mainly through their small size and surface reactivity, which promote cellular uptake and the generation of reactive oxygen species (ROS).

The release of silver ions (Ag^+) from the nanoparticles further enhances toxicity by interacting with cellular machinery and triggering inflammatory responses [74, 75]. Cytotoxic effects depend on factors such as particle size with smaller particles being more toxic dose, exposure time, shape, and surface chemistry, as well as the cell type, with cancer cells often being more sensitive [76]. These toxic effects extend to the environment where AgNPs impact soil and aquatic organisms through oxidative stress and ionic silver release, disrupting growth, reproduction, and enzyme activity, raising concerns about ecological safety and prompting exploration of mitigation strategies like phytoremediation [77]. Phytochemical components such as flavonoids, phenolic acids, terpenoids, saponins, polysaccharides, alkaloids, proteins, and

reducing sugars play crucial roles in the green synthesis of AgNPs. These plant-derived metabolites act effectively as reducing agents by donating electrons or hydrogen atoms to reduce silver ions (Ag^+) to metallic silver (Ag^0) [38].

Flavonoids and polyphenols, known for their hydroxyl groups, are particularly efficient in this reduction process. Besides reduction, many phytochemicals serve as stabilizing and capping agents that adhere to the nanoparticle surfaces, preventing aggregation and enhancing nanoparticle stability [39]. The dual role of these biomolecules not only facilitates eco-friendly synthesis but also imparts beneficial biological properties to AgNPs. Green synthesis using plant extracts is considered environmentally friendly and cost-effective, producing stable nanoparticles suitable for diverse applications. These phytochemicals are key to controlling nanoparticle size, shape, and stability in green synthesis methods [40]. *Rhubarb* is a therapeutic plant rich in bioactive constituents such as flavonoids, tannins, glycosides, anthraquinones, volatile oils, and saponins. These compounds exhibit diverse biological activities, including antibacterial, antifungal, antioxidant, and anticancer effects, along with immune-boosting and wound-healing properties [41]. New materials in wastewater treatment are revolutionizing the field by combining nanotechnology, advanced membranes, and smart composites. These materials offer high efficiency in removing a wide range of contaminants including organic pollutants, heavy metals, and pathogens while improving sustainability through reusability and reduced chemical use [65, 66].

Notably, membrane bioreactors integrated with nanocomposite membranes are enhancing filtration performance and fouling resistance, allowing for effective treatment and potential water reuse. Additionally, stimuli-responsive biomaterials and metal-organic frameworks contribute to selective removal and adaptability in treatment processes, making them promising candidates for industrial and municipal wastewater applications [67, 68]. Current research likely formulates a focused set of hypotheses regarding (i) the dual role of *Rhubarb* seed extract in reducing and capping silver nanoparticles to produce bio-synthesized AgNPs with enhanced surface functionality. (ii) the research aims to explore the synergistic mechanism by which these biogenic AgNPs and the *Rhubarb*-derived matrix selectively adsorb and catalytically degrade organic dyes. (iii) it seeks to determine the applicability of standard isotherm and kinetic models in distinguishing between adsorption and catalytic degradation contributions. The originality of this research lies in connecting plant-mediated biosynthesis parameters to quantitative adsorption and degradation behavior within a single framework. This approach allows for a deeper understanding of how surface chemistry and defect functionality imparted by the plant extract influence dye removal efficiency, rate, and potential mineralization. By offering a green synthesis route with a clear, model-based interpretation of performance, this work distinguishes between adsorption-dominated uptake and catalytic pathways. It also provides a predictive method for adjusting dye removal efficiency across various dye classes. To the best of our knowledge, no reported report on the green synthesis of AgNPs using *Rhubarb* seed extract. Hence, the present study aimed to present a simple, green, low-cost, and fast method for the synthesis of AgNPs using *Rhubarb* seed extract and its application there to removal of MB, MO, and AR18 from aqueous environments. The effects of important parameters such as pH, adsorbent dosage, contact time, and initial dye concentration on the dye removal efficiency were studied. Isotherm and kinetic models were used to interpret the adsorption process. Furthermore, this study presents a green and environmentally friendly synthesis of silver nanoparticles using *Rhubarb* seed extract as a bio-reductant and natural stabilizer. This innovative approach eliminates the dependence on harmful chemicals and energy-intensive processes common in conventional methods. The biogenic AgNPs demonstrate effective catalytic properties in removing harmful organic dyes from aqueous solutions, addressing critical environmental pollution. The research provides a comprehensive analysis of adsorption mechanisms through detailed studies of isotherm and kinetic models, which reveal the adsorption capacity, efficiency, and dynamics involved in the dye degradation process. Moreover, it addresses the gap of limited studies using *Rhubarb* seed extract in the biosynthesis of silver nanoparticles for organic dye removal. It makes a novel contribution by integrating a green synthesis approach with a detailed adsorption isotherm and kinetics model. This helps elucidate the mechanistic interactions and optimize the efficiency of AgNPs in wastewater treatment. By integrating sustainable nanomaterial synthesis with practical wastewater treatment applications and rigorous model-based evaluation, this work advances both green nanotechnology and environmental remediation techniques.

10.57647/jnsc.2026.1601.03

2. Materials and methods

2.1. Materials

Silver nitrate ($AgNO_3$) of 99.95% purity, along with MB, MO, and AR18, was acquired from Merck (Germany). *Rhubarb* seeds were sourced from Alborz Province.

2.2. Preparation of *Rhubarb* seed extract

Rhubarb seed extract was prepared using a method outlined in a previously published article in the literature [69]. *Rhubarb* seeds (10 g) were ground and combined with 100 mL of distilled water. The solution was stirred on a heated stirrer at 70 °C for 2 h. Afterwards, the extract was separated by filtration through Whatman No. 14 filter paper.

2.3. Green synthesis of AgNPs

AgNPs were green-synthesized according to a previously published article in the literature [70]. A mixture of 100 mL of 0.01 M $AgNO_3$ and 10 mL of seed extract was stirred at 600 rpm for 24 h at ambient temperature. AgNPs were formed when a dark-brown color change was observed. The solution was then subjected to multiple centrifugation cycles at 5000 rpm for 15 min each. This solution was heated at 60 ◦C for 6 h to obtain a dried product.

2.4. Adsorption experiments

Adsorption experiments are crucial for evaluating adsorbents and their effectiveness in removing pollutants. Kinetic and isotherm data were collected during the experiments to assess the removal of dye pollutants MB, MO, and AR18. The chemical structures of all three studied dyes are illustrates in Scheme 1. This was done by adding a measured amount of adsorbent to a 100 mL flask containing a known concentration of contaminants. Initially, the adsorbent was mixed with the contaminant solution, and the experiment was conducted on a shaker for up to 50 min. An ultrasonic homogenizer was also utilized to prevent particle aggregation and colloid formation during the adsorption studies. Samples were taken from the mixture at specific intervals, and the adsorbent particles were then separated from the liquid phase through centrifugation. In all experiments, the adsorbent dosage was 0.8 g. This research utilized the one-factor-at-a-time (OFAT) method to remove MB, MO, and AR18 dyes using synthesized AgNPs. The experimental conditions pH (3–12), adsorbent dosage (0.1–0.8 g), contact time (5–30 min), and initial concentration (20–60 mg/L) were investigated. Subsequently, a Shimadzu UV-1800 double-beam UV–Vis spectrophotometer was used to record the adsorption spectra of the samples, measuring absorbance at the respective maximum wavelengths for methylene blue (664 nm)[71], methyl orange (465 nm)[72], and acid red 18 (506 nm) [73] Each experiment was repeated three times, and the average was considered at the end.

The removal efficiency was calculated as follows (Eq. 1):

$$Removal(\%) = \frac{C_0 - C_e}{C_0} \times 100 \qquad (1)$$

Where C_0 and C_e (mg/L) are the initial and final dye concentrations, respectively [42].

3. Results and Discussion

3.1. Characterization of biosynthesized AgNPs

3.1.1. *Naked-eye observation and UV–Vis spectroscopy*

The synthesis of AgNPs was characterized by a color change from colorless to dark brown within 24 h (Fig 1a).

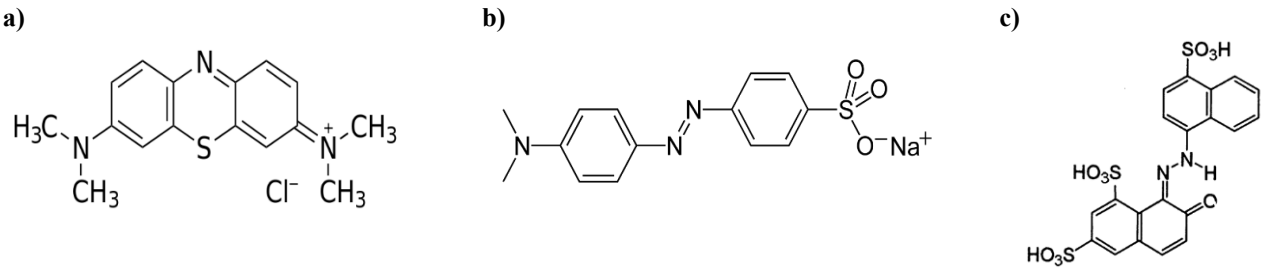

Scheme 1. (a), The chemical structure of (a) MB, (b) MO, and (c) AR18

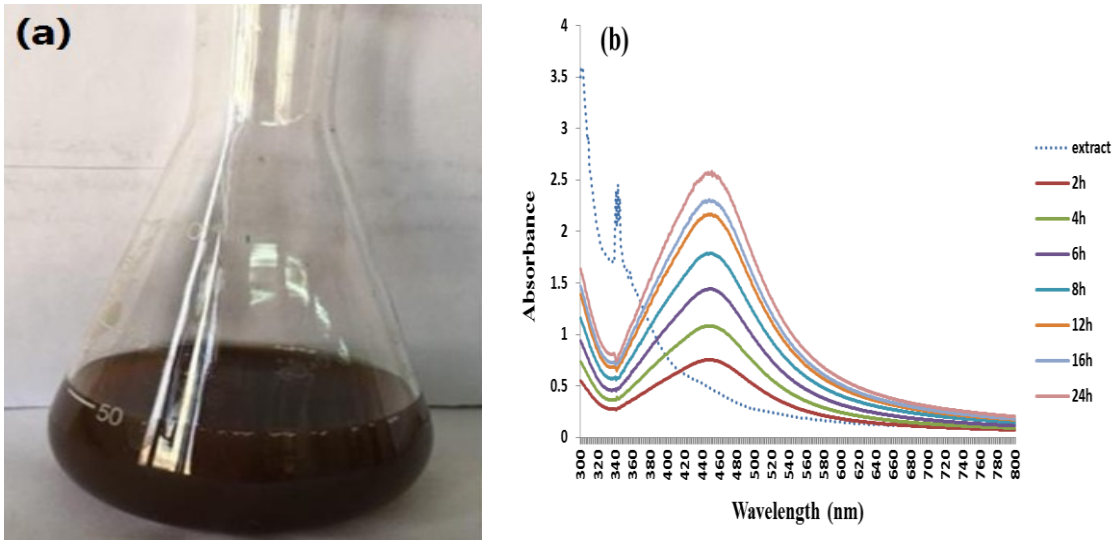

Figure 1. (a) The Dye of AgNPs after 24 h and (b) the UV-Vis spectra of biosynthesized AgNPs obtained at various reaction durations

An optical characteristic named surface plasmon resonance (SPR), which is found in noble metals, leads to this color change [30]. Moreover, UV-Vis spectroscopy verified the formation of AgNPs, with adsorption was recorded over the range of 300–800 nm (Fig 1b). The extract exhibited a peak at a wavelength of 343 nm, which was related to the adsorption of the formation of the extract using the biosynthesis method. After the reduction of $AgNO_3$ using the extract, AgNPs exhibited adsorption peaks at approximately 450 nm at different reaction times, which were assigned to the SPR of AgNPs, indicating the success of the process. Extending the reaction time from 2 to 24 h led to a stronger SPR peak observed at 451 nm. In addition, the peak broadening at a contact time of 24 h indicates the synthesis of AgNPs with larger sizes [4].

To estimate the optical band gap energy through UV-Vis absorption spectrum analysis, the band gap of the materials plays a crucial role in photocatalysis. The differences in absorbance among various catalysts indicate varying band gaps. The relevant band gap energies of the nanoparticles can be determined using the Tauc equation (Eq. 2) [89].

$$\alpha h\nu = A(h\nu - E_g)^n \quad (2)$$

Absorption coefficient (α); hν: Photon energy in eV, calculated as hν = 1240/λ (λ in nm); Eg: Band gap energy; n: 1/2 for direct allowed transitions, sometimes 2 for indirect; A and n are constants. The band gap of the optical nature of prepared samples was calculated by extrapolating the linear portion of hν versus $(\alpha h\nu)^2$ plots to the hν axis. Photon energy at the edge: hν = 1240/450 ≈ 2.76 eV. In practice, the linear region in the Tauc plot (2.5–3.5 eV range) extrapolates to Eg ≈ 2.8–3.2 eV for biogenic AgNPs with SPR ~420 nm. A specific estimate for this system is Eg ≈ 3.0 eV (direct band gap). This estimate comes from typical values for *Rhubarb*-extract AgNPs, where the organic capping narrows the gap slightly from pure Ag (~3.5 eV effective) due to plasmonic enhancement. A 3.0 eV gap means strong UV absorption (λ < 413 nm), generating electron-hole pairs that produce reactive oxygen species (ROS) for dye degradation.

3.1.2. *TEM and DLS analysis*

The morphology and particle size distribution of the biosynthesized AgNPs were studied using Zeiss TEM 10C-1000Kv (Germany) and dynamic light scattering (DLS), respectively. TEM confirmed the spherical shape of the AgNPs (Fig 2a). The TEM image reveals that biosynthesized AgNPs are predominantly spherical and well-dispersed, with moderate agglomeration and diameters mostly below 20 nm. The accompanying particle size distribution histogram shows a narrow, nearly Gaussian profile, peaking around 10–11 nm (Fig 2b).

This indicates that most particles fall within 6–12 nm, confirming the successful synthesis of uniformly sized AgNPs with minimal size variation factors. These factors are crucial for applications requiring small, monodisperse nanomaterials such as catalysis, antimicrobial actions, or sensing [81]. The formation of spherical nanoparticles could be attributed to the interactions among biomolecules present in the *Rhubarb* seed extract [35].

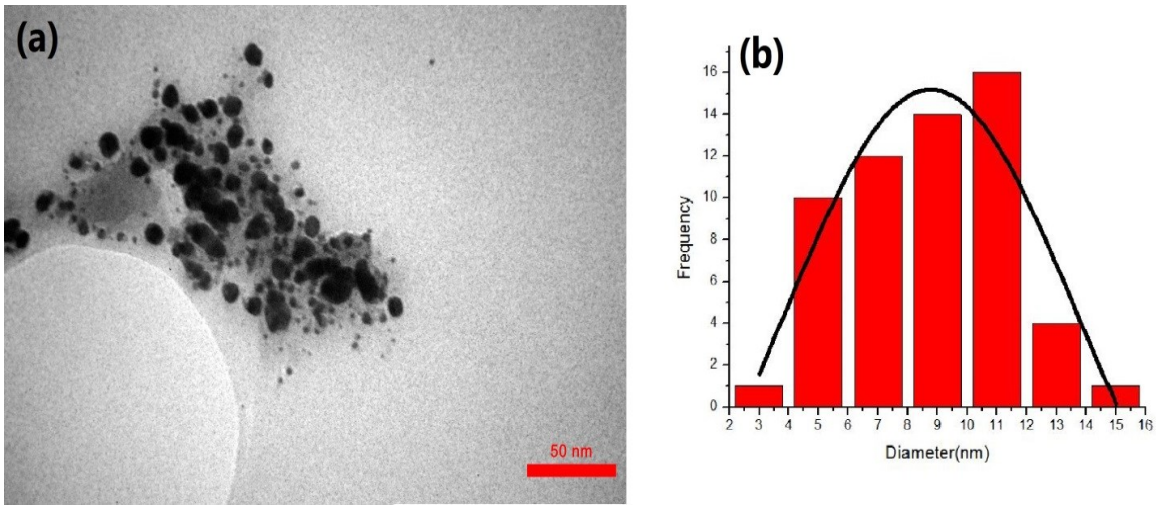

Figure 2. (a) TEM image and (b) particle size distribution of AgNPs

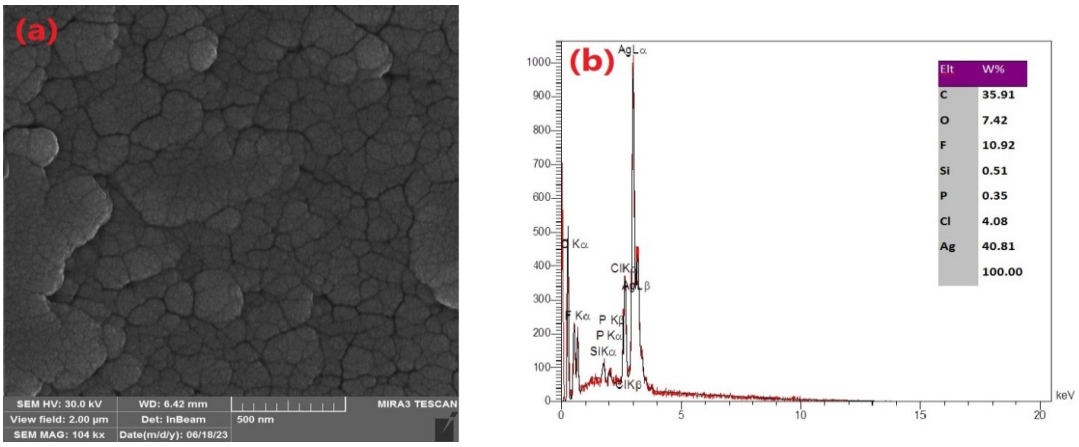

Figure 3. (a) SEM image and (b) EDX spectrum of biosynthesized AgNPs.

3.1.3. SEM and EDX analysis

A SEM Zeiss Sigma 500 VP was employed to examine the form and surface features of the biosynthesized AgNPs. The biosynthesized AgNPs with a generally spherical shape and some degree of aggregation, indicating effective nanoparticle formation and stabilization by biological agents (Fig 3a). Coating agents, such as organic molecules, may have caused NP aggregation [43]. The elemental makeup of the biosynthesized AgNPs was analyzed through EDX spectroscopy. The accompanying EDX spectrum confirms a high silver content (40.81 wt%), with additional minor elements such as carbon, oxygen, fluorine, and chlorine, which originate from organic biomolecules and precursors used during biosynthesis, suggesting successful reduction and capping of AgNPs (Fig 3b). This peak appeared at approximately 3 keV owing to the SPR phenomenon [44]. There are carbon (C) and oxygen (O) peaks with weights of 35.91% and 7.42%, respectively, which can be attributed to the presence of C–C, C–H, C–OH, C=O, and C–O–C [35]. These signals in the EDX profile may also be caused by biomolecules attached to the surface of the AgNPs [87]. This combination of SEM and EDX analysis verifies the formation, purity, and bio-organic nature of AgNPs synthesized through a green route.

3.1.4. FTIR analysis

The functional groups of the extract and produced AgNPs were analyzed with a PerkinElmer Spectrum 100 FTIR spectrophotometer (USA) using KBr pellets over the 4000–400 cm^{-1} range which is illustrates in Fig. 4 spectra of Rhubarb seed extract and biosynthesized AgNPs using seed extract. The major absorption peak in the seed extract appeared at 3417 cm^{-1} which is related to the O-H stretching vibration. The weak peak around 2900 cm^{-1} is due to the stretching vibration of C-H [36]. The peak at 1617 cm^{-1} can be assigned to the stretching vibrations of the aliphatic C=C group [34]. The C–N stretching vibration is observed at 1352 cm^{-1} [40,45]. The sharp peak at 1026 cm^{-1} is ascribed to C-O-C and secondary OH groups [46].

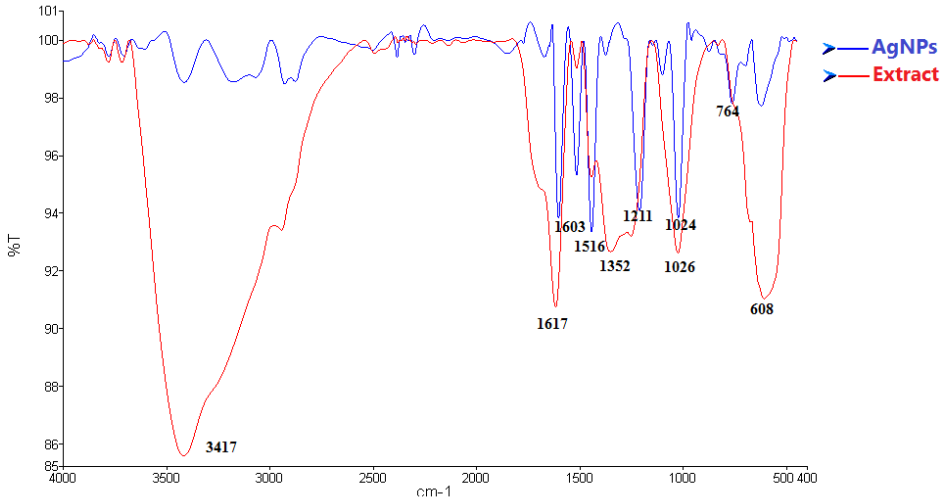

Figure 4. FTIR spectra of *Rhubarb* seed extract and biosynthesized AgNPs using seed extract

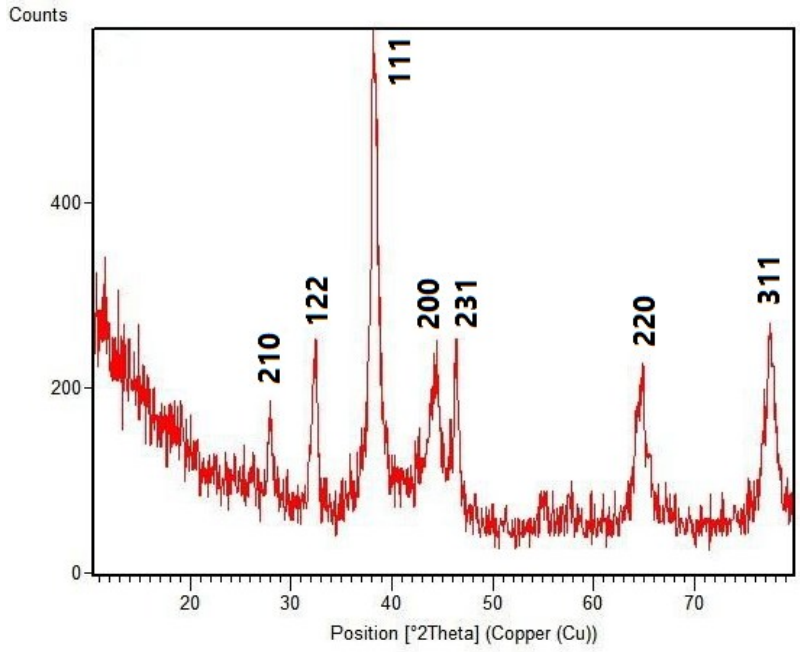

Figure 5. XRD pattern of biosynthesized AgNPs using seed extract

The peak detected at 608 cm^{-1} is attributed to the C–Cl stretching vibration within the alkyl group [44]. Some of the peaks of the seed extract were shifted in the synthesized AgNPs, such as 1617 cm^{-1} to 1603 cm^{-1} and 1026 cm^{-1} to 1024 cm^{-1}. The peak observed at 1211 cm^{-1} corresponds to the C-N stretching vibration of the amine group [42]. The bending vibration of N-H appears at 1516 cm^{-1} [33].

3.1.5. XRD analysis

Malvern Panalytical XRD with Cu-Ka radiation with 2θ values ranging from 10◦ to 80◦ was used to study the crystalline nature of biosynthesized AgNPs (Fig 4). Bragg reflections appeared at 2 equal of 27.96◦, 32.45◦, 38.17◦, 44.26◦, 46.37◦, 64.64◦, and 77.59◦, which can be assigned to the (210), (122), (111), (200), (231), (220), and (311) planes, respectively (Fig 5). The reported values closely match those provided by the Joint Committee on Powder Diffraction Standards (JCPDS), Card No. 04-0783, for silver with a face-centered cubic (FCC) structure [34,47]. The average crystallite size (Dp) of the biosynthesized AgNPs can be calculated using Debye–Scherrer (Eq. 3) [88]:

$$D_p = \frac{K\lambda}{\beta\, cos\theta} \quad (3)$$

Where Dp is the crystallite size of materials, θ is half of Bragg's angle in degrees, β is the corrected

half of the diffraction peak in radians, λ= 0.15406 nm is the X-ray wavelength for CuKα source, and k is a crystallite shape factor usually taken as 0.94. For the characteristic peaks at 27.96◦, 32.45◦, 38.17◦, 44.26◦, 46.37◦, 64.64◦, and 77.59◦, Dp was calculated to be 5.12, 8.79, 11.58, 13.25, 14.88, 16.34, and 19.40, respectively. This indicates that the biosynthesized AgNPs have an average size of 12.22 nm. XRD analysis is utilized to evaluate the stability of silver nanoparticles biosynthesized through the adsorption process by examining the crystallinity and structural integrity of the particles. Stable AgNPs generally exhibit sharp characteristic peaks in the XRD pattern at positions corresponding to the (111), (200), (220), and (311) planes of the FCC structure. The lack of peak broadening or shifts after adsorption indicates that the nanoparticles remain crystalline, unaggregated, and structurally stable, making them suitable for repeated dye removal applications [78].

3.2. The effect of different factors on the removal of dyes

3.2.1. The effect of pH

One of the important factors influencing the adsorption of dyes onto AgNPs is the pH of the solution. (Fig 6a) shows the effect of pH on the removal of MB, MO, and AR18. By dissolving MB as a basic dye in water, positively charged ions are generated. Therefore, as the pH of the dye solution increases, the electrostatic attraction between the positively charged dye and the negatively charged adsorbent due to the presence of functional groups such as amino and hydroxyl groups occurs [6,7]. The maximum percentage removal (96.83%) of MB by AgNPs was related to a pH of 11. As shown, by increasing the pH from 3 to 9, the removal efficiency was enhanced from 33.62% to 96.88%. Increasing the pH beyond this point did not result in a notable difference in removal efficiency. Methyl orange is an anionic dye bearing a negative charge. Under acidic conditions, hydronium ions predominate and can occupy vacant adsorbent surface sites, while the positively charged sites attract MO molecules. As the pH increased, the number of positively charged sites on the adsorbent decreased. Therefore, a significant increase in the adsorption of MO molecules on the adsorbent surface was observed with increasing pH [11]. Silver nanoparticles release silver ions (Ag^+) during the adsorption process primarily through surface oxidation, facilitated by their small size and high surface area. This accelerates ion dissolution compared to bulk silver. Initially, ion leaching occurs rapidly, but then slows as the nanoparticles age or degrade [61]. Environmental factors such as pH, oxygen, and light further influence the rate of ion release. The released silver ions contribute to the antimicrobial and adsorptive properties of AgNPs but also pose potential toxicity risks in aqueous environments. The presence of an oxide layer on AgNPs can control the rate of ion release, balancing efficacy and stability during adsorption [62]. The maximum removal efficiency of AR18 dye (96.79%) occurred at pH 5, likely due to the abundance of positive charges on the adsorbent surface and the negatively charged AR18 molecules under acidic conditions, promoting electrostatic attraction and enhancing pollutant uptake [2].

3.2.2. The effect of adsorbent dosage

One of the most important factors in studying the pollutant removal process is investigating the optimal dosage of adsorbent for maximum adsorption and removal efficiency. In this research, the impact of varying adsorbent amounts on the removal of MB, MO, and AR18 was assessed by introducing different adsorbent weights into 100 ml of pollutant-containing solution, while keeping other variables constant. The surface active sites of the adsorbent significantly influence the elimination of dye pollutants from wastewater. The balance of the adsorbate-adsorbent is determined by the amount of adsorbent, and with its help, it is possible to predict the cost of treatment in the desired system [11]. The effect of adsorbent dosage on the removal of the specified dyes was examined within the range of 0.1 to 0.8 g (Fig 6b). The removal efficiency rose as the adsorbent dosage increased from 0.1 to 0.8 g, due to the greater available surface area and number of active sites, but subsequently declined as the surface became saturated [13].

3.2.3. The effect of contact time

The impact of contact time critically influences the evaluation of adsorbent performance. Accordingly, the adsorption of MB, MO, and AR18 by the synthesized materials was tested over a period of 5–30 min under constant room temperature conditions. Contact time was investigated over the range of 5 to 30 min, with the maximum removal efficiency (exceeding 95%) achieved at 20 min for all dyes (Fig 6c). The adsorption of all three dyes consisted of two phases. In the initial stage, adsorption proceeds

rapidly due to the large number of vacant active sites on the adsorbent surface available for dye molecule interaction. In the second phase, the adsorption rate is slower because the available active sites are reduced, which tends to slow down the adsorption process and then becomes constant [1,3].

3.2.4. *The effect of initial concentration*

The impact of initial concentration on removal efficiency was examined using various concentrations in a 100 mL solution containing dye contaminants. The removal efficiency at variable dye concentrations (20-60 mg/L) was assessed (Fig 6d). The removal percentage increased with dye concentration up to 30 mg/L. Furthermore, an increase in dye concentration led to a decrease in the removal efficiency.

At low concentrations, empty active sites are present on the adsorbent surface [6]. As the initial dye concentration increased, the removal percentage gradually decreased, possibly due to the saturation of the available active sites [47]. Therefore, an initial concentration of 30 mg/L was chosen as optimal, achieving a maximum removal efficiency greater than 96%.

3.3. Adsorption isotherm

This study evaluated the experimental results using two isotherm models, Langmuir and Freundlich. According to the Langmuir model, adsorption takes place uniformly at active sites on the adsorbent surface, where interactions between adsorbate molecules prevent the formation of multilayer coverage, resulting in a single adsorbed layer. The linear Langmuir isotherm can be expressed as follows (Eq. 4):

$$\frac{C_e}{q_e} = \frac{1}{q_m K_L} + \frac{C_e}{q_m} \quad (4)$$

Where C_e (mg/L) and q_e (mg/g) denote the adsorbate concentration and adsorption capacity at equilibrium, respectively. K_L (L/g) and q_m (mg/g) are assigned to the Langmuir adsorption energy constant and the maximum adsorption capacity, respectively, which were calculated by plotting C_e/q_e versus C_e (Fig 7a) using the slope and intercept values of the linear equation [48].

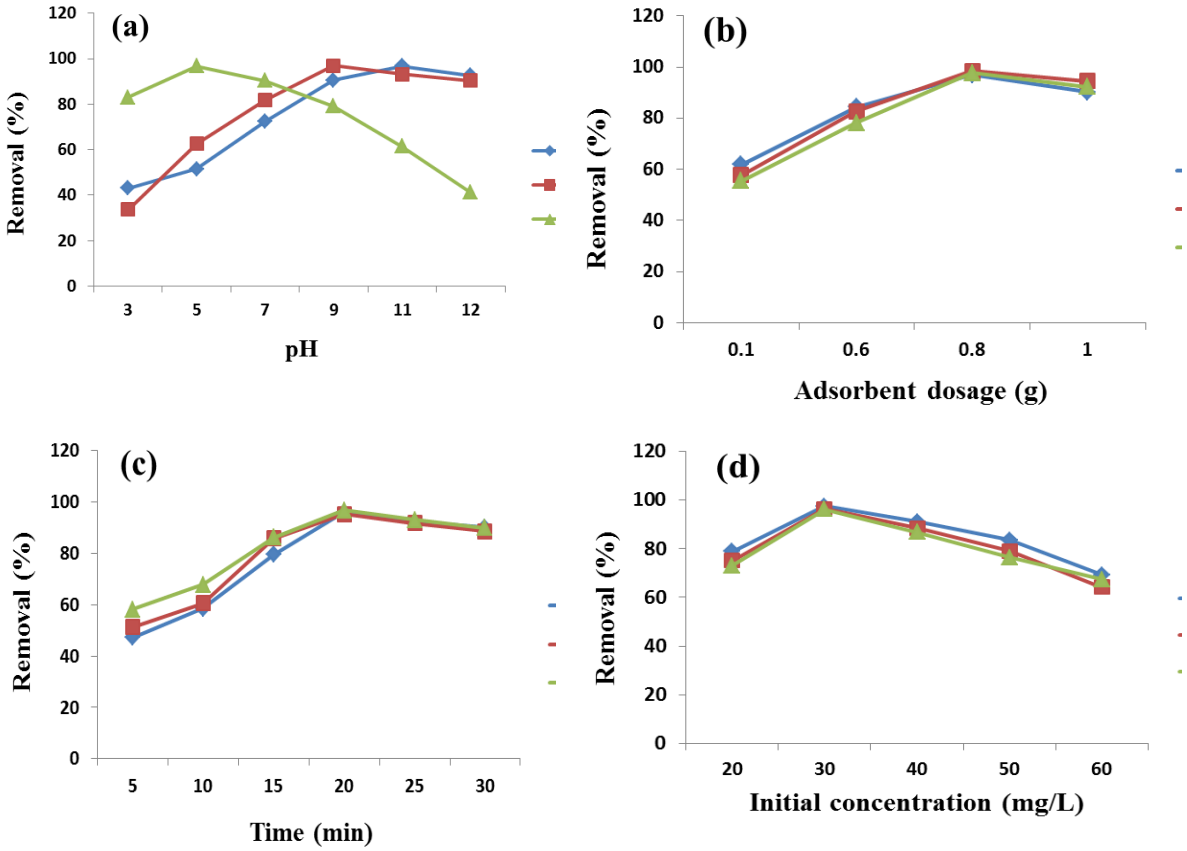

Figure 6. The impact of (a) pH, (b) adsorbent amount, (c) contact duration, and (d) starting concentration on the removal efficiency of MB, MO, and AR18 was evaluated

The q_{max} values of the biosynthesized AgNPs for the adsorption of MB, MO, and AR18 were 40.16, 50.76, and 44.64 mg/g, respectively. The close alignment of the experimental results with the Langmuir model suggests a constant, dimensionless separation factor (R_L) (Eq. 5).

$$R_L = \frac{1}{1 + K_L C_0} \quad (5)$$

Herein, the maximum initial concentration of the pollutant and the adsorption nature are demonstrated by C_0 (mg/L) and RL, respectively. The irreversible, favorable, linear, and unfavorable adsorption is specified by $R_L = 0$, $0 < R_L < 1$, $R_L = 1$, and $R_L > 1$, respectively [49]. The R_L values for MB, MO, and AR18 were 0.2687, 0.06737, and 0.1233, respectively, demonstrating favorable monolayer adsorption.In contrast, the Freundlich model can describe heterogeneous surfaces and multilayer adsorption processes, and its linear form is shown in (Eq. 6).

$$\log q_e = \log\ (K_F) + \frac{1}{n} \log\ (C_e) \quad (6)$$

Where K_F and 1/n represent the constant parameters related to the adsorption capacity and intensity of the adsorption, respectively, which were determined using the slope and intercept of the log q_e versus log C_e plot (Fig 7b) [50]. The results revealed that 1/n for all three dyes was less than 1 (MB=0.4542, MO=0.3900, AR18=0.4889), which proves the desirability of adsorbing the dyes on the adsorbent, and n greater than 1 show that the processes are physical. In addition, a higher K_F value indicates better adsorption [51]. Table 1 presents the calculated parameter values for both isotherm models applied to the three dyes. Due to the larger coefficient of determination (R^2) of the Langmuir isotherm, it can be said that the adsorption of dyes follows this isotherm.

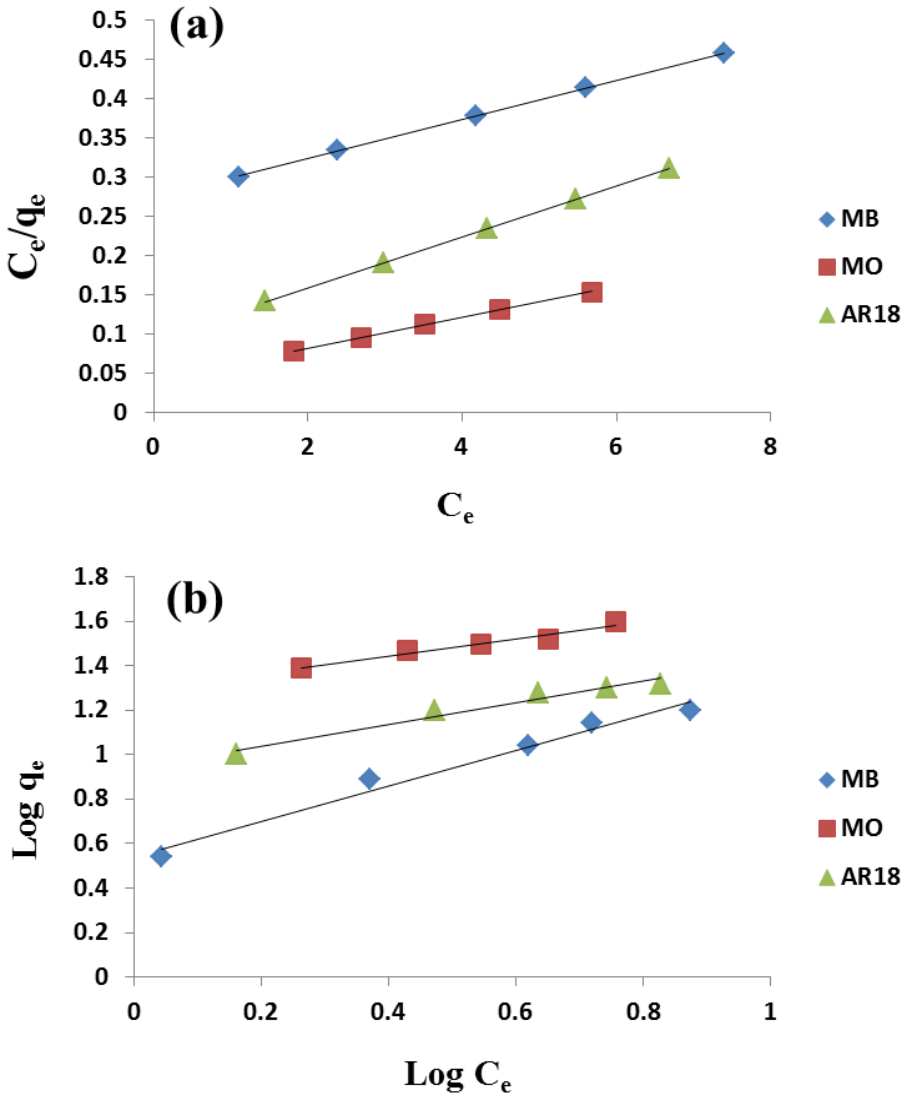

Figure 7. (a) Langmuir and (b) Freundlich adsorption models applied to the removal of MB, MO, and AR18 with biosynthesized AgNPs

Table 1. Parameters derived from isotherm models for the removal of MB, MO, and AR18

Isotherms	Parameters	MB	MO	AR18
Langmuir	q_m *(mg/g)*	40.16	50.76	44.64
	K_L *(L/mg)*	9068	0.4614	0.237
	R^2	0.9998	0.9994	0.9995
	R_L	2687	0.06737	1233
Freundlich	K_F *(mg/g).(L/mg)*$^{1/n}$	5.497	19.48	8.757
	1/n	4542	0.39	4889
	R^2	0.9775	0.9581	0.9619

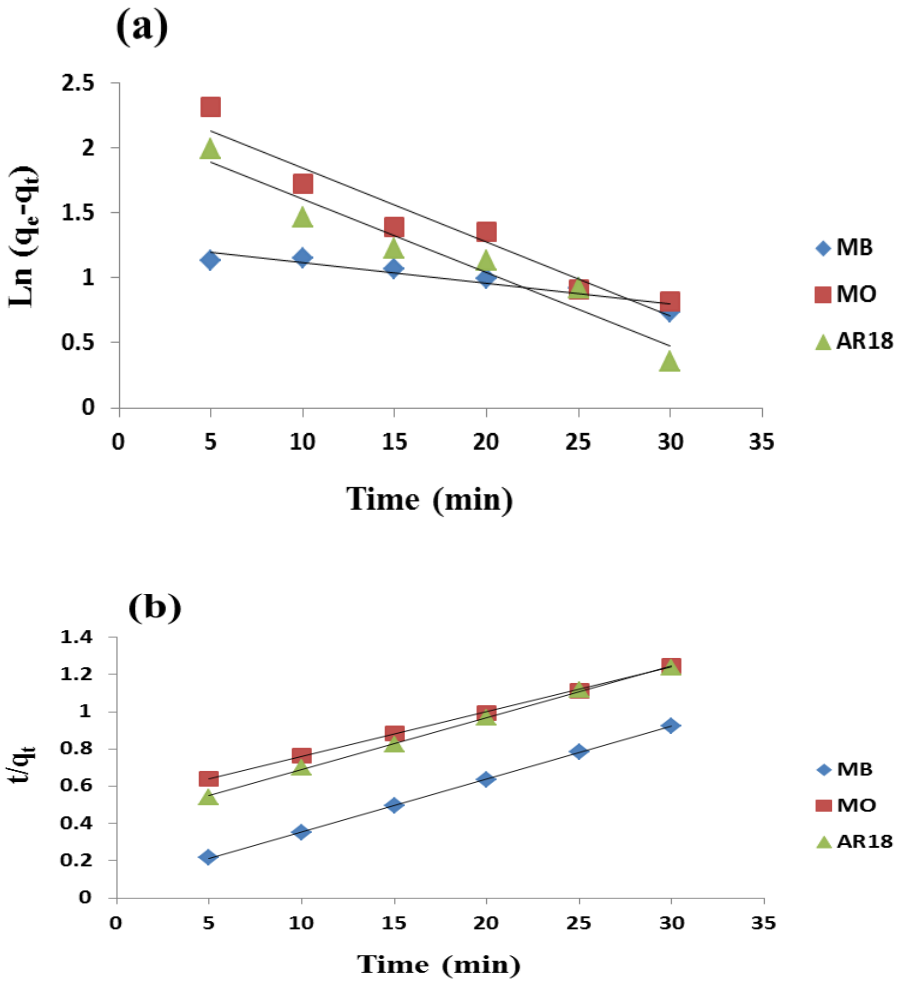

Figure 8. (a) Pseudo first-order and (b) Pseudo second-order kinetic models for the adsorption of MB, MO, and AR18 with biosynthesized AgNPs

Table 2. Kinetic parameters obtained for the removal of MB, MO, and AR18

Kinetic	Parameters	MB	MO	AR18
Pseudo-first-order	k_1 *(1/min)*	0.0159	0.057	0.0567
	q_e *(cal) (mg/g)*	3.59	11.21	8.788
	R^2	0.8948	0.9325	0.9388
Pseudo-second-order	k_2 *(g/mg.min)*	0.0111	1.11×10^{-3}	1.90×10^{-3}
	q_e *(cal) (mg/g)*	35.33	41.66	35.84
	R^2	0.9998	0.9992	0.9991

10.57647/jnsc.2026.1601.03

3.4. Kinetic study

Adsorption kinetics are essential in designing any adsorption system because they predict the rate of adsorption in a specific setup. Pseudo-first-order (PFO) and pseudo-second-order (PSO) kinetics are suitable for dye removal because they account for the main rate-controlling steps typically seen in adsorption systems: external diffusion and surface interactions (PFO) versus chemisorption or surface-reaction processes (PSO) [58]. In practice, many dye-adsorbent systems exhibit rapid initial uptake that corresponds to PFO under diffusion-limited conditions, followed by slower phases that are better described by PSO when chemical interactions or strong binding at active sites determine the long-term approach to equilibrium [59]. When PSO provides a better fit (and the derived q_e matches experimental values), it suggests chemisorption or strong adsorbate-surface interactions. An improvement in fit quality for PFO at early times indicates initial diffusion-controlled uptake. Kinetic models like pseudo-first-order (PFO) and pseudo-second-order (PSO) are commonly applied to assess the adsorption rate and identify the controlling step. The mathematical form of the PFO model is given by (Eq. 7):

$$\ln(q_e - q_t) = \ln q_e - k_1(t) \quad (7)$$

In this context, q_e (mg/g) represents the amount of pollutant adsorbed at equilibrium, q_t (mg/g) is the dye adsorption amount at time t (min), and k_1 (1/min) denotes the adsorption rate constant. The k_1 and q_e values were found from the slope and intercept of the graph of Ln (q_e–q_t) versus time as given in (Fig 8a). The PSO kinetic model can be expressed using (Eq. 8).

$$\frac{t}{q_t} = \frac{1}{k_2 q_e^2} + \frac{t}{q_e} \quad (8)$$

Where the second-order adsorption rate constant is denoted by k_2 (g/mg.min). The parameters q_e and k_2 can be determined from the slope and intercept of the plot of t/q_t against time (Fig 8b) [52]. The estimated parameters are presented in Table 2. The R^2 values of PSO models for three dyes are higher than PFO, which shows that the data match with the PSO model.

3.5. Adsorption mechanism

The adsorption mechanism involves the accumulation of molecules on a surface due to unbalanced surface forces, resulting in physical or chemical interactions. The fundamental adsorption mechanism is influenced by the adsorbent's characteristics, such as surface area, functional groups, pore structure, and optimal conditions [55]. To determine the adsorption mechanism of MB, MO, and AR18 based on the results obtained from the AgNPs adsorbent the proposed adsorption mechanisms were identified. The proposed mechanism scheme, as shown in Fig 9, illustrates the adsorption of MB, MO, and AR18 by AgNPs. An electrostatic interaction between the functional groups of AgNPs with the negative charge and the positive charge (N^+) in the MB structure occurs [1]. The justification for adsorption of MB onto AgNPs based adsorbents biosynthesized from *Rhubarb* seed involves a combination of surface interactions and nanoparticle-mediated processes. In this context, MB adsorption can be driven by electrostatic attraction, chemical interactions with surface functionalities, and, in some systems, catalytic or reductive pathways that accompany adsorption. Below is a structured justification framework you can apply to study results from *Rhubarb* seed derived AgNP adsorbents [56, 57]. The effect of electrostatic interactions and hydrogen bonds can describe the adsorption mechanism of MO on the surface of AgNPs. The surface of biosynthesized AgNPs possesses some different functional groups. MO molecules can bind to those groups such as OH [12]. There is a positive charge on the surface of AgNPs at low pH solutions and electrostatic attraction between AgNPs and opposing charges of AR18 molecules is created, which leads to increased dye removal [16]. In order to propose a mechanism for the photocatalytic degradation of dye molecules by nanocomposites, a study conducted by M.K.H. Shishir et al.[60] (2026) aimed to confirm the degradation pathway and the extent of mineralization after irradiation. The nanocomposite adsorbs light and generates electron-hole pairs. These charge carriers produce reactive oxygen species (-OH, O_2^-) that attack dye molecules, breaking chromophores and aromatic rings, leading to intermediates and ultimately mineralization to CO_2 and H_2O. The presence of heterogeneous junctions, plasmonic components, or defect sites enhances charge separation and radical formation, accelerating the degradation process. Verification should include the identification of intermediates, Total Organic Carbon (TOC) analysis for mineralization, radical trapping experiments to confirm active species, and surface analyses (FTIR/XPS) to observe bond changes and ensure that the observed dye loss is related to true mineralization and not simply decolorization.

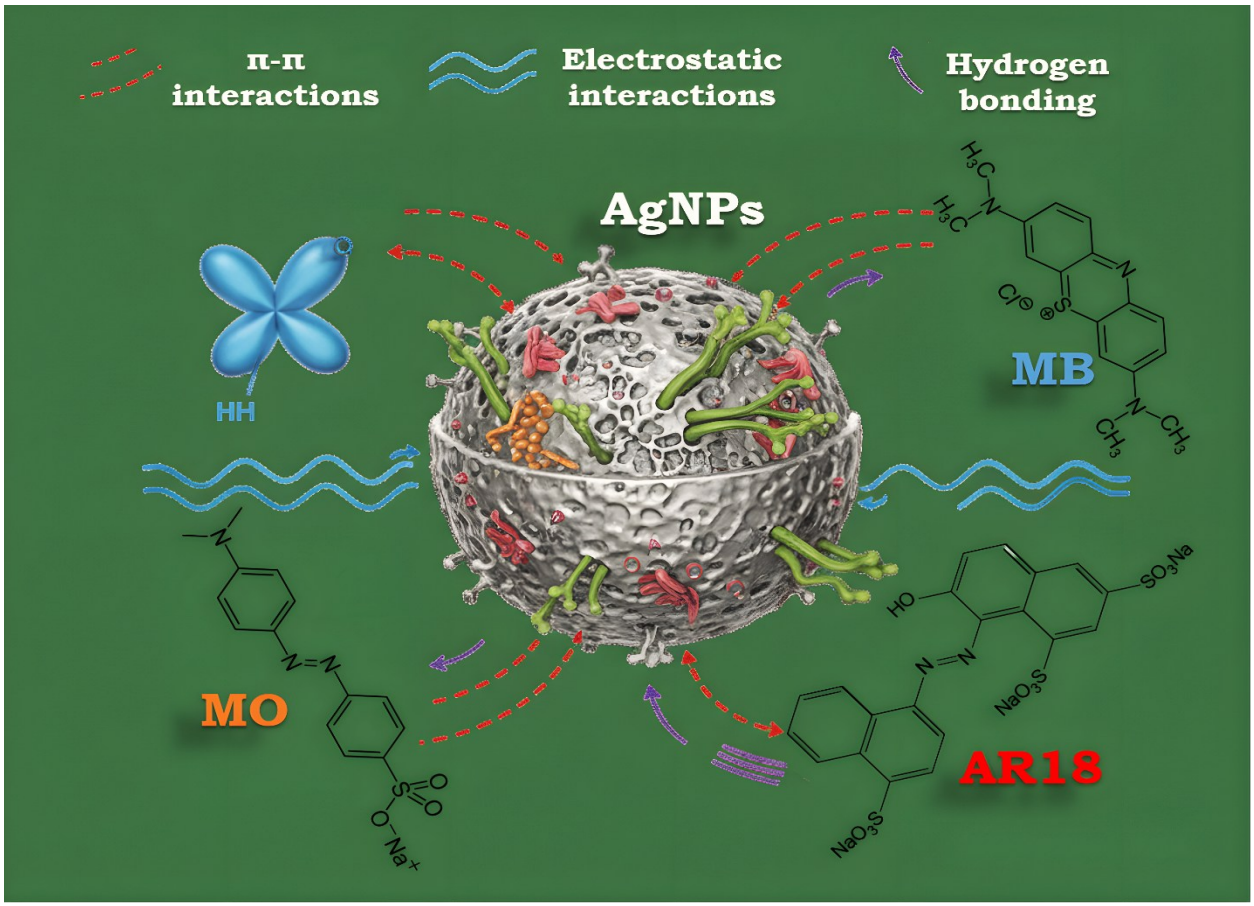

Figure 9. Schematic diagram of the possible adsorption mechanism of MB, MO, and AR18 on AgNPs

The porous structure of AgNPs, combined with their surface chemistry, creates a synergistic effect that significantly enhances the removal of dyes from water. AgNPs provide a high surface area and tailored pore size, offering abundant adsorption sites and facilitating interactions through hydrogen bonding with dye molecules. Meanwhile, they contribute diverse surface functional groups and additional porosity, strengthening adsorption through π-π interactions and electrostatic interactions. Together, these materials form a composite that maximizes adsorption capacity and efficiency, enabling the effective removal of dyes. This makes it a promising material for water purification applications.

3.6. Comparative study

Table 3 displays the maximum adsorption capacity (q_{max}), removal efficiency, and contact time of biosynthesized AgNPs in this study in comparison with other adsorbents for the removal of MB, MO, and AR18 (Table 3). Two adsorbents activated carbon developed by *Ficus carica* bast and Anchote peel show a higher adsorption capacity compared to the present study because they had a higher contact time. The q_{max} values and percentage removal of other adsorbents even with higher contact time are lower than those reported for biosynthesized AgNPs using *Rhubarb* seed extract. The results demonstrated the high efficiency of the proposed green adsorbent compared to other adsorbents. The biosynthesized AgNPs exhibit excellent adsorption performance due to their relatively large particle sizes (about 30-70 nm), negative surface charge, and bio-functional groups from natural capping agents such as flavonoids and proteins that enhance stability and pollutant binding. These green-synthesized AgNPs display strong surface plasmon resonance and spherical morphology, facilitating hydrophobic interactions, hydrogen bonding, and electrostatic interactions with pollutants. This contributes to effective adsorption and catalytic degradation of dyes like methylene blue [63]. Compared to chemically synthesized or other nanoparticle systems, biosynthesized AgNPs demonstrate competitive or superior adsorption efficiency.

This is thanks to eco-friendly synthesis routes that impart additional functional groups and surface reactivity, ensuring rapid adsorption kinetics and eco-compatible pollutant removal. This validates their novelty and significance in environmental remediation applications [64].

10.57647/jnsc.2026.1601.03

Table 3. Comparison of adsorption capacities of various adsorbents for the removal of MB, MO, and AR18

Adsorbent	Dyes	q_{max} (mg/g)	Removal efficiency (%)	Time (min)	Ref.
AgNPs/ functionalized-silica	Indigo Carmine (IC)	73.05	96.38	20	[82]
AgNPs loaded on Chitosan (AgCS)	MB	---	>70	120	[83]
AgNPs/GO	MB	---	98	<5	[84]
Ag^0	MB	---	100	10	[85]
Solanum tuberosum peel (STpe)-AgNP	Bromophenol Blue (BB)	9.604	88.5	120	[86]
AgNPs	MB	40.16	>95.00	20	Present study
AgNPs	MO	50.76	>95.00	20	Present study
AgNPs	AR18	44.64	>95.00	20	Present study

4. Conclusion

This research presents an eco-friendly method for producing AgNPs utilizing *Rhubarb* seed extract. Characterization of fabricated biosynthesized AgNPs was accomplished using UV-Vis spectrophotometer, TEM, SEM, XRD, FTIR, and EDX. The ability of the AgNPs to remove MB, MO, and AR18 was investigated in batch studies with different experimental parameters, including the solution pH, adsorbent dosage, contact time, and initial dye concentration. The adsorption follows the Langmuir isotherm model and adheres to pseudo-second-order kinetics. The proposed method does not require organic solvents and surfactants, so it is nature-friendly. Furthermore, this method is cost-effective, simple, and rapid with high efficiency for the removal of MB, MO, and AR18 from aqueous media. The results indicate that biosynthesized AgNPs are effective and promising adsorbents for removing various dyes from industrial wastewater.

Declaration of competing interest
The authors declare that they have no known competing financial interests or personal relationships that could have appeared to influence the work reported in this paper.

Acknowledgement
The authors would like to appreciate the technical support provided by the Islamic Azad University of Islamshahr, Iran.

Funding statements
There is no funding used for this research.

Data availability
Data will be made available on request.

References

[1] Singh, C. K., Sodhi, K. K., N. V., Rajagopalan, V., Sharma, S., Kaur, J., Kumar, Y. Managing the complexity of emerging contaminants in aquatic environments: exploring their ecotoxicological impacts, detection techniques, and the use of innovative technologies for their remediation. *Discov Catal* **2**, 9 (2025).

[2] Khan, W. U., Ahmed, S., Dhoble, Y., Madhav, S. A critical review of hazardous waste generation from textile industries and associated ecological impacts. *J Indian Chem Soc* **100**, 100829 (2023).

[3] Sarwar, T., Khan, S. 2022. Textile industry: pollution health risks and toxicity. *In Textile Wastewater Treatment: Sustainable Bio-nano Materials and Macromolecules*, pp. 1–28. Springer Nature, Singapore.

[4] Rabeie, B., Mahmoodi, N. M. Environmentally friendly novel covalent organic framework composites as porous photocatalysts and adsorbents for tetracycline and dyes (Congo red and methylene blue) removal: green synthesis, kinetics, regeneration, and removal mechanisms. *Appl Mater Today* **46**, 102884 (2025).

[5] Benosmane, N., Boutemeur, B., Hamdi, S. M., Hamdi, M. Removal of methylene blue dye from aqueous solutions using polymer inclusion membrane technology. *Appl Water Sci* **12**, 104 (2022).

[6] Mehta, J., Dhaka, R. K., Dilbaghi, N., Lim, D. K., Hassan, A. A., Kim, K. H., Kumar, S. Recent advancements in adsorptive removal of organophosphate pesticides from aqueous phase using nanomaterials. *J Nanostruct Chem* **14**, 53–70 (2024).

[7] Agnihotri, S., Sillu, D., Sharma, G., Arya, R. K. Photocatalytic and antibacterial potential of silver nanoparticles derived from pineapple waste: process optimization and modeling kinetics for dye removal. *Appl Nanosci* **8**, 2077–2092 (2018).

[8] Din, M. I., Khalid, R., Hussain, Z., Arshad, M., Khan, S. A. A critical review on application of organic, inorganic and hybrid nanophotocatalytic assemblies for photocatalysis of methyl orange dye in aqueous medium. *Rev Chem Eng* **40**, 67–91 (2024).

[9] Hanafi, M. F., Sapawe, N. A review on the water problem associated with organic pollutants derived from phenol, methyl orange, and Remazol Brilliant Blue dyes. *Mater Today* **31**, A141–A150 (2020).

[10] Thamaraiselvi, C., Athira, S. T., & Vasanthy, M. Sustainable management of coffee cherry pulping wastewater using biogenically synthesized calcium oxide nanoparticles. *Next Mater* **10**, 101393 (2026).

[11] Abdisa Hambisa, A., Biyana Regasa, M., Gurmessa Ejigu, H., & Boru Senbeto, C. Adsorption studies of methyl orange dye removal from aqueous solution using Anchote peel based agricultural waste adsorbent. *Appl Water Sci*, **12**, 24 (2023).

[12] Estefan, E., Elystia, S., Kuan, W. H., & Sasmita, A. Removal of methyl orange textile dye using magnetic chitosan microspheres adsorbent. *Water Pract Technol*, **18**, 3280–3290 (2023).

[13] Naseer, A. Role of nanocomposites and nano adsorbents for heavy metals removal and dyes: An overview. *Desalin Water Treat*, **320**, 100662 (2024).

[14] Ramesh, H., & Bhuyan, A. K. Food Colorants Acid Yellow 23, Azorubine, and Acid Red 18 Cause Aggregation and Fibrillation of Proteins. *ACS Food Sci Technol*, **4**, 963–974 (2024).

[15] Khan, R. R. M., Qamar, H., Hameed, A., Rehman, A. U., Pervaiz, M., Saeed, Z., Adnan, A., & Ch, A. R. Biological and photocatalytic degradation of Congo red, a diazo sulfonated substituted dye: A review. *Water Air Soil Pollut*, **233**, 468 (2022).

[16] Saini, R., & Choudhary, K. 2025. Toxic potential of Azo dyes: A broader understanding. *In Hazardous Chemicals*, pp. 469–481. Academic Press.

[17] Li, T., Wei, L., Fang, Y., Cui, Y., Wang, X., & Li, Y. Risk identification of human health, ecotoxicity, and degradation products of azo dyes: development of a priority control list. *Environ Pollut*, **386**, 127180 (2025).

[18] Ramamurthy, K., Priya, P. S., Murugan, R., & Arockiaraj, J. Hues of risk: investigating genotoxicity and environmental impacts of azo textile dyes. *Environ Sci Pollut Res*, **31**, 33190–33211 (2024).

[19] Ahmed, H. M., Fawzy, M. E., & Nassar, H. F. Effective chemical coagulation treatment process for cationic and anionic dyes degradation. *Egypt J Chem*, **65**, 299–307 (2022).

[20] Mohamed Noor, M. H., & Ngadi, N. Ecotoxicological risk assessment on coagulation-flocculation in water/wastewater treatment: a systematic review. *Environ Sci Pollut Res*, **31**, 52631–52657 (2024).

[21] Amri, N., Zuhairi Abdullah, A., & Ismail, S. Removal efficiency of Acid Red 18 dye from aqueous solution using different aluminium-based electrode materials by electrocoagulation process. *Indones J Chem*, **20**, 536–544 (2020).

[22] Akter, S., & Islam, S. Effect of additional Fe2+ salt on electrocoagulation process for the degradation of methyl orange dye: an optimization and kinetic study. *Heliyon*, **8**, e10176 (2022).

[23] Tap Van, H., Hung Hoang, V., Cuc Luu, T., Linh Vi, T., Thi Quynh Nga, L., Ivan Jimenez Marcaida, G. S., & Phamgh, T. T. Enhancing acid orange II degradation in ozonation processes with CaFe2O4 nanoparticles as a heterogeneous catalyst. *RSC Adv*, **13**, 28753–28766 (2023).

[24] Siagian, U. W., Khoiruddin, K., Wardani, A. K., Aryanti, P. T., Widiasa, I. N., Qiu, G., Ting, Y. P., & Wenten, I. G. High-performance ultrafiltration membrane: recent progress and its application for wastewater treatment. *Curr Pollut Rep*, **7**, 448–462 (2021).

[25] Kathing, C., & Saini, G. A review of various treatment methods for the removal of dyes from textile effluent. *Recent Prog Mater*, **4**, 4 (2022).

[26] Esfandiaribayat, M., Binazadeh, M., Sabbaghi, S., Mohammadi, M., Ghaedi, S., & Rajabi, H. Tetracycline removal from wastewater via g-C3N4 loaded RSM CCD optimised hybrid photocatalytic membrane reactor. *Sci Rep* **14**, 1163 (2024).

[27] Dinarvand, H., & Moradi, O. Sustainable approaches for pharmaceutical pollutant removal: advances in chitosan-based nanocomposite adsorbents. *ChemistrySelect* **10**, e202405962 (2025).

[28] Kocaman, S. Removal of methylene blue dye from aqueous solutions by adsorption on levulinic acid-modified natural shells. *Int J Phytoremediation* **22**, 885–895 (2020).

[29] El Messaoudi, N., El Khomri, M., El Mouden, A., Bouich, A., Jada, A., Lacherai, A., Iqbal, H. M., Mulla, S. I., Kumar, V., & Américo-Pinheiro, J. H. P. Regeneration and reusability of non-conventional low-cost adsorbents to remove dyes from wastewaters in multiple consecutive adsorption–desorption cycles: a review. *Biomass Conv Bioref* **14**, 11739–11756 (2024).

[30] Jasrotia, T., Dhiman, N., Sharma, N., Singh, A., Chaudhary, S., Chaudhary, G. R., & Kumar, R. Biomonitoring and risk assessment of naturally and chemically synthesized iron-oxide nanoparticles: a comparative approach. *Sci Total Environ* **872**, 161960 (2023).

[31] Tesfaye, M., Gonfa, Y., Tadesse, G., Temesgen, T., & Periyasamy, S. Green synthesis of silver nanoparticles using Vernonia amygdalina plant extract and its antimicrobial activities. *Heliyon* **9**, e17356 (2023).

[32] Yadav, J., & Chauhan, P. Green synthesis of silver nanoparticles using Citrus X sinensis (orange) fruit extract and assessment of their catalytic reduction. *Mater Today Proc* **62**, 6177–6181 (2022).

[33] de Souza, T. A. J., Souza, L. R. R., & Franchi, L. P. Silver nanoparticles: an integrated view of green synthesis methods, transformation in the environment, and toxicity. *Ecotoxicol Environ Saf* **171**, 691–700 (2019).

[34] Singh, H., Desimone, M. F., Pandya, S., Jasani, S., George, N., Adnan, M., Aldarhami, A., Bazaid, A. S., & Alderhami, S. A. Revisiting the green synthesis of nanoparticles: uncovering influences of plant extracts as reducing agents for enhanced synthesis efficiency and its biomedical applications. *Int J Nanomedicine*, 4727–4750 (2023).

[35] Varshney, S., Verma, S., & Gupta, A. Valorization of the halo-alkaliphilic bacterial culture supernatant of Nesterenkonia lacusekhoensis EMLA3 for sustainable silver nanoparticles synthesis: insights into catalytic dye removal, antibacterial activity, and phytotoxicity of treated wastewater. *Mater Sci Eng B* **323**, 118785 (2026).

[36] Yadav, S., Nadar, T., Lakkakula, J., & Wagh, N. S. 2024. Biogenic synthesis of nanomaterials: bioactive compounds as reducing, and capping agents. *In Biogenic Nanomaterials for*

Environmental Sustainability: Principles, Practices, and Opportunities, pp. 147–188. Springer.

[37] Rani, G., Bala, A., Ahlawat, R., Nunach, A., & Chahar, S. Recent advances in synthesis of AgNPs and their role in degradation of organic dyes. *Comments Inorg Chem* **45**, 1–29 (2025).

[38] Fahim, M., Shahzaib, A., Nishat, N., Jahan, A., Bhat, T. A., & Inam, A. Green synthesis of silver nanoparticles: a comprehensive review of methods, influencing factors, and applications. *JCIS Open* **16**, 100125 (2024).

[39] Gwada, C. A., Ndivhuwo, P. S., Matshetshe, K., Aradi, E., Mdluli, P., Moloto, N., & Airo, M. Phytochemical-assisted synthesis, optimization, and characterization of silver nanoparticles for antimicrobial activity. *RSC Adv* **15**, 14170–14181 (2025).

[40] Bragta, D., Garg, P., Chaudhary, S., Madhok, G., Negi, S., Panwar, S. et al. Eco-friendly biosynthesis of ZnO nanoparticles using fungus Schizophyllum commune and their hybrid with chitosan for enhanced UV-A photocatalytic degradation of tetracycline. *Chemosphere* **387**, 144666 (2025).

[41] Kolodziejczyk-Czepas, J., & Liudvytska, O. Rheum rhaponticum and Rheum rhabarbarum: a review of phytochemistry, biological activities and therapeutic potential. *Phytochem Rev* **20**, 589–607 (2021).

[42] Pirkarami, A., & Olya, M. E. Removal of dye from industrial wastewater with an emphasis on improving economic efficiency and degradation mechanism. *J Saudi Chem Soc* **21**, S179–S186 (2017).

[43] Chouhan, S., & Guleria, S. Green synthesis of AgNPs using Cannabis sativa leaf extract: characterization, antibacterial, anti-yeast and α-amylase inhibitory activity. *Mater Sci Energy Technol* **3**, 536–544 (2020).

[44] De Barros, C. H. N., Cruz, G. C. F., Mayrink, W., & Tasic, L. Bio-based synthesis of silver nanoparticles from orange waste: effects of distinct biomolecule coatings on size, morphology, and antimicrobial activity. *Nanotechnol Sci Appl*, 1–14 (2018).

[45] Ider, M., Abderrafi, K., Eddahbi, A., Ouaskit, S., & Kassiba, A. Silver metallic nanoparticles with surface plasmon resonance: synthesis and characterizations. *J Clust Sci* **28**, 1051–1069 (2017).

[46] Ahmad, R., & Ejaz, M. O. Adsorption of methylene blue dye from aqueous solution onto synthesized bentonite/silver nanoparticles-alginate (Bent/AgNPs-Alg) bio-nanocomposite. *Biomass Conv Bioref* **14**, 27061–27076 (2024).

[47] Hieu, N. H., Duyen, D. T. M., Thang, T. Q., Duy, P. H. A., Lam, H. D. N., Phat, L. N., & Phong, M. T. Fabrication of reduced graphene oxide-doped carbon aerogels from water hyacinth for removal of methylene blue in water and energy storage. *J Nanostruct Chem* **14**, 383–401 (2024).

[48] Grace Femi-Adepoju, A., Oluwasogo Dada, A., Opeyemi Otun, K., Olufemi Adepoju, A., & Paul Fatoba, O. Green synthesis of silver nanoparticles using terrestrial fern (Gleichenia pectinata (Willd.) C. Presl.): characterization and antimicrobial studies. *Heliyon* **5**, e01543 (2019).

[49] Singh, H., Raghuvanshi, R. S., Singh, A., Talla, M. K., Ali, S., Chauhan, R., & Gautam, D. Adsorption efficacy of silver nanoparticles synthesized using wintergreen plant extract: a green approach to dye removal. *Colloid J* **2025**, 1–13 (2025).

[50] Sevim, F., Lacin, O., Ediz, E. F., & Demir, F. Adsorption capacity, isotherm, kinetic, and thermodynamic studies on adsorption behavior of malachite green onto natural red clay. *Environ Prog Sustainable Energy* **40**, e13471 (2021).

[51] Paredes-Quevedo, L. C., González-Caicedo, C., Torres-Luna, J. A., & Carriazo, J. G. Removal of a textile azo-dye (Basic Red 46) in water by efficient adsorption on a natural clay. *Water Air Soil Pollut* **232**, 4 (2021).

[52] Na, C. Size-controlled capacity and isocapacity concentration in Freundlich adsorption. *ACS Omega* **5**, 13130–13135 (2020).

[53] Tolkou, A. K., Mitropoulos, A. C., & Kyzas, G. Z. Removal of anthraquinone dye from wastewaters by hybrid modified activated carbons. *Environ Sci Pollut Res* **30**, 73688–73701 (2023).

[54] Dal, M. C., & Onursal, N. Two new linearized equations derived from the pseudo-second-order kinetic model. *Desalin Water Treat* **308**, 183–189 (2023).

[55] Nayak, A., Bhushan, B., & Kotnala, S. 2024. Fundamentals and mechanism of adsorption. *In Sustainable Remediation Technologies for Emerging Pollutants in Aqueous Environment*, pp. 29–62. Elsevier.

[56] Bencheikh, I., Azoulay, K., Mabrouki, J., El Hajjaji, S., Dahchour, A., Moufti, A., & Dhiba, D. The adsorptive removal of MB using chemically treated artichoke leaves: parametric, kinetic, isotherm and thermodynamic study. *Sci Afr* **9**, e00509 (2020).

[57] Bai, R., Feng, Y., Wu, L., Li, N., Liu, Q., Teng, Y. et al. Adsorption mechanism of methylene blue by magnesium salt-modified lignite-based adsorbents. *J Environ Manage* **344**, 118514 (2023).

[58] Revellame, E. D., Fortela, D. L., Sharp, W., Hernandez, R., & Zappi, M. E. Adsorption kinetic modeling using pseudo-first order and pseudo-second order rate laws: a review. *Clean Eng Technol* **1**, 100032 (2020).

[59] Rudzinski, W., & Plazinski, W. Kinetics of solute adsorption at solid/solution interfaces: a theoretical development of the empirical pseudo-first and pseudo-second order kinetic rate equations, based on applying the statistical rate theory of interfacial transport. *J Phys Chem B* **110**, 16514–16525 (2006).

[60] Shishir, M. K. H., Akand, M. S., Maola, M., Monira, M. F., Rifat, M., Sayeem, N. R., & Khan, G. M. A. Photocatalytic removal of textile dyes: analytical strategies for post-degradation evaluation. *Desalination* **617**, 119437 (2026).

[61] Agnihotri, S., Mukherji, S., & Mukherji, S. Immobilized silver nanoparticles enhance contact killing and show highest efficacy: elucidation of the mechanism of bactericidal action of silver. *Nanoscale* **5**, 7328–7340 (2013).

[62] Pongkitdachoti, U., & Unob, F. Simultaneous adsorption of silver nanoparticles and silver ions on large pore mesoporous silica. *J Environ Chem Eng* **6**, 596–603 (2018).

[63] Shahzadi, S., Fatima, S., Shafiq, Z., & Janjua, M. R. S. A. A review on green synthesis of silver nanoparticles (SNPs) using plant extracts: a multifaceted approach in photocatalysis, environmental remediation, and biomedicine. *RSC Adv* **15**, 3858–3903 (2025).

[64] Vorobyova, V., Vasyliev, G., Uschapovskiy, D., Lyudmyla, L., & Skiba, M. Green synthesis, characterization of silver nanoparticles for biomedical application and environmental remediation. *J Microbiol Methods* **193**, 106384 (2022).

[65] Oviedo, L. R., Durzian, D. M., Montagner, G. E., Ruiz, Y. P. M., Galembeck, A., Pavoski, G., & da Silva, W. L. Supported heterogeneous catalyst of the copper oxide nanoparticles and nanozeolite for binary dyes mixture degradation: machine learning and experimental design. *J Mol Liq* **402**, 124763 (2024).

[66] Da Silva, W. L., Lansarin, M. A., dos Santos, J. H. Z., Da Rocha, Z. N., & Pepe, I. M. Electrochemical and catalytic studies of a supported photocatalyst produced from petrochemical residue in the photocatalytic degradation of dexamethasone and guaifenesin drugs. *Water Air Soil Pollut* **227**, 242 (2016).

[67] da Silva, M. D. C. R., Druzian, D. M., Brum, L. F. W., dos Santos, C., Pavoski, G., Espinosa, D. C. R., & da Silva, W. L. Green synthesis of ZrO2/PdO-NPs for photodegradation of anionic dyes: photocatalytic activity and machine learning modelling. *J Mol Liq* **410**, 125581 (2024)

[68] Wouters, R. D., Druzian, D. M., Muraro, P. C. L., Da Silva, M. D. C. R., Dos Santos, C., Ruiz, Y. P. M., & Da Silva, W. L. TiO2-NPs/ZnO-NPs@ Co3O4 nanocomposite from natural extracts for the Rhodamine 6 G photodegradation. *Surfaces Interfaces* **48**, 104282 (2024).

[69] Tan, L., Geng, D. D., Hu, F. Z., & Dong, Q. Rapid identification and quantification of natural antioxidants in the seeds of Rhubarb from different habitats in China using accelerated solvent extraction and HPLC-DAD-ESI–MSn-DPPH Assay. *J Chromatogr Sci* **54**, 48–57 (2016).

[70] Ghaffari-Moghaddam, M., Hadi-Dabanlou, R., Khajeh, M., Rakhshanipour, M., & Shameli, K. Green synthesis of silver nanoparticles using plant extracts. *Korean J Chem Eng* **31**, 548–557 (2014).

[71] Fernández-Pérez, A., & Marbán, G. Visible light spectroscopic analysis of methylene blue in water. *J Appl Spectrosc* **88**, 1284–1290 (2022).

[72] Wu, L., Liu, X., Lv, G., Zhu, R., Tian, L., Liu, M., Li, Y., Rao, W., & Liu, T. Study on the adsorption properties of methyl orange by natural one-dimensional nano-mineral materials with different structures. *Sci Rep* **11**, 10640 (2021).

[73] Shirmardi, M., Mesdaghinia, A., Mahvi, A. H., Nasseri, S. et al. Kinetics and equilibrium studies on adsorption of Acid Red 18 (Azo-dye) using multiwall carbon nanotubes (MWCNTs) from aqueous solution. *J Chem* **9**, 2371–2383 (2012).

[74] Brum, L. F. W., da Silva, M. D. C. R., dos Santos, C. et al. Green synthesis of niobium (V) oxide nanoparticles using pecan nutshell (Carya illinoinensis) and evaluation of its antioxidant activity. *Catal Today* **445**, 115106 (2025).

[75] Pinheiro, L. D. S. M., Sangoi, G. G., Vizzotto, B. S. et al. Silver nanoparticles from ascorbic acid: biosynthesis, characterization, in vitro safety profile, antimicrobial activity and phytotoxicity. *Mater Chem Phys* **325**, 129715 (2024).

[76] Pinheiro, L. D. S. M., Sangoi, G. G., Righi, N. C. et al. PLA/PCL polymer nanocomposite with silver and copper nanoparticles and lavender essential oil: synthesis, characterization and application in tissue engineering. *Surfaces Interfaces* **55**, 105391 (2024).

[77] de Menezes, L. B., Druzian, D. M., Oviedo, L. R. et al. In vitro safety profile and phyto-ecotoxicity assessment of the eco-friendly calcium oxide nanoparticles. *Chemosphere* **365**, 143407 (2024).

[78] Elmehalawy, N. G., Zaky, M. M., Eid, A. M. & Fouda, A. Eco-friendly synthesis of silver nanoparticles: multifaceted antioxidant, antidiabetic, anticancer, and antimicrobial activities. *Sci Rep* **15**, 37349 (2025).

[79] Hijazi, B. U., Faraj, M., Mhanna, R. & El-Dakdouki, M. H. Biosynthesis of silver nanoparticles as a reliable alternative for the catalytic degradation of organic dyes and antibacterial applications. *Curr Res Green Sustainable Chem* **8**, 100408 (2024).

[80] Sati, A., Ranade, T. N., Mali, S. N. et al. Silver nanoparticles (AgNPs): comprehensive insights into bio/synthesis, key influencing factors, multifaceted applications, and toxicity—a 2024 update. *ACS Omega* **10**, 7549–7582 (2025).

[81] Hegazy, M. A. & Borham, E. Preparation and characterization of silver nanoparticles homogenous thin films. *NRIAG J Astron Geophys* **7**, 27–30 (2018).

[82] Gemeay, A. H., Aboelfetoh, E. F. & El-Sharkawy, R. G. Immobilization of green synthesized silver nanoparticles onto amino-functionalized silica and their application for indigo carmine dye removal. *Water Air Soil Pollut* **229**, 16 (2018).

[83] Sultan, M., Siddique, M., Khan, R. et al. Ligustrum lucidum leaf extract-assisted green synthesis of silver nanoparticles and nano-adsorbents having potential in ultrasound-assisted adsorptive removal of methylene blue dye from wastewater and antimicrobial activity. *Materials* **15**, 1637 (2022).

[84] Rohaizad, A., Shahabuddin, S., Shahid, M. M. et al. Green synthesis of silver nanoparticles from Catharanthus roseus dried bark extract deposited on graphene oxide for effective adsorption of methylene blue dye. *J Environ Chem Eng* **8**, 103955 (2020).

[85] Saha, J., Begum, A., Mukherjee, A. & Kumar, S. A novel green synthesis of silver nanoparticles and their catalytic action in reduction of Methylene Blue dye. *Sustainable Environ Res* **27**, 245–250 (2017).

[86] Akpomie, K. G. & Conradie, J. Biogenic and chemically synthesized Solanum tuberosum peel–silver nanoparticle hybrid for the ultrasonic aided adsorption of bromophenol blue dye. *Sci Rep* **10**, 17094 (2020).

[87] Alam, M. Analyses of biosynthesized silver nanoparticles produced from strawberry fruit pomace extracts in terms of biocompatibility, cytotoxicity, antioxidant ability, photodegradation, and in-silico studies. *J King Saud Univ Sci* **34**, 102327 (2022).

[88] Islam, K. S., Mustak, M. H., Shishir, M. K. H. et al. Biosynthesis of ZnO nanoparticles using banana peel pectin for antibacterial and photocatalytic applications. *S Afr J Chem Eng* **52**, 127–140 (2025).

[89] Bayzid, T., Shishir, M. K. H., Akand, M. S. et al. Crystallographic analysis of silk sericin-stabilized zinc oxide nanoparticles with enhanced antimicrobial and photocatalytic properties. *Inorg Chem Commun* **178**, 114481 (2025).